Available online at www.sciencedirect.com
ScienceDirect
Progress in Solid State Chemistry 36 (2008) 192–212
Progress in Solid State Chemistry
www.elsevier.com/locate/pssc

Hydrogen insertion effects on the magnetic properties and chemical bonding within C14 Laves phases

A.F. Al Alam [a], S.F. Matar [a,*], N. Ouaïni [b], M. Nakhl [b]

[a] *CNRS, ICMCB, University of Bordeaux, 33608 Pessac, France*
[b] *Faculty of Science and Engineering, Holy Spirit University of Kaslik, Jounieh, Lebanon*

Abstract

The Laves phases family, AB_2 ($A = 3_B$, 4_B, rare earth or actinide; B = transition metal) is among the largest of binary intermetallic systems. They readily absorb hydrogen and as such they are of potential use for energy storage. This work presents a thorough electronic and magnetic structure study within these systems among which we select $ScFe_2$ and its hydride $ScFe_2H_2$ which crystallize in the C14 (2H) hexagonal structure. The relevance of this study for solid state chemistry pertains to the complexity brought by the presence of two distinct crystal sites for Fe with different magnetic properties (ordered moments, hyperfine fields) and bonding with hydrogen whose insertion sites were to be defined. Such issues, not considered experimentally, are addressed here within the well-established quantum mechanical density functional theoretical framework (DFT) using both pseudo-potential calculations for geometry optimization and all-electrons investigations for full study of the electronic, chemical bonding and magnetic structure properties. From energy–volume quadratic curves providing the equation of state, the hydride is found more compressible at a higher equilibrium volume than the pristine intermetallic. This stresses the negative pressure brought by hydrogen. Cohesive energy studies show the stability of hydrogen within $ScFe_2$. From electron localization function (ELF) plots the expected picture of a negatively charged hydrogen within an alloy lattice is obtained. The chemical bond of H within the *A*2*B*2 tetrahedron formed of Sc and one type of Fe is discussed. Magnetic moments and Fermi contact term H_{FC} of the effective hyperfine field H_{eff} are found within range of the average experimental values in both the alloy and its hydride. For $ScFe_2H_2$ a peculiar feature of the magnetic moment magnitude inversion

* Corresponding author. Fax: +33 5 4000 2761.
E-mail address: matar@icmcb-bordeaux.cnrs.fr (S.F. Matar).

0079-6786/$ - see front matter © 2008 Elsevier Ltd. All rights reserved.
doi:10.1016/j.progsolidstchem.2008.07.001

and of H_{FC} for the two iron sites is found to be connected with a change in magnetic characters of the two Fe sites, becoming strongly and weakly ferromagnetic, respectively, for the isolated iron and the H connected Fe.
© 2008 Elsevier Ltd. All rights reserved.

Keywords: DFT; C14 Laves phases; Hydrides; Magnetic orders; ASW; VASP; Hyperfine field

Contents

1. Introduction

Binary alloys belonging to the Laves family AB_2 ($A = 3_B$, 4_B, rare earth or actinide; B = transition metal) crystallize either in a face centered cubic (fcc) (C15) lattice or in a hexagonal lattice (C14); further, dihexagonal (C36) minority structure exists [1,2]. These intermetallic systems readily absorb hydrogen in large amounts, up to 6 H per formula unit (fu) [3–5]. Besides the large potential applications of Laves phases' hydrides in the field of solid

state storage of hydrogen for energetics [6,7], there is a basic interest in studying the changes of the magnetic structure and of the electronic properties due to H insertion. One of its main issues is to identify the origin of the magnetism which can be either due to the transition metal or induced by the A metal, depending on the bonding nature of the involved species [8,9].

Within the Laves family, $ScFe_2$ exhibits polymorphism and can exist in the above three crystalline states. Nevertheless, experimental studies [10] report the formation of a more stable C14 structure below 1473 K with respect to less stable C15 and C36 structures at higher temperatures, i.e., at 1798 K and above 1473 K. Laves intermetallic phases are usually in the C14 (2H) hexagonal form and transformation to C15 (3C) form is slow, requiring long sintering periods at elevated temperatures. A mechanism based on X-ray investigations, propose a germination and propagation of stacking faults leading to plane gliding in the solid state from 2H to 3C structures for systems other than AB_2 ones [11]. This was later extended to, and detailed for, the polytipic transformations in Laves phases with the so-called synchroshear transformation mechanism based on observations made by atomic resolution microscopy [12]. Among others [10,13], Smit and Buschow have studied the synthesis of C14-type $ScFe_2$ and its corresponding hydride system $ScFe_2H_2$ [3]. An interesting structural peculiarity is that Fe is found in two distinct sublattices which are likely to interact differently with interstitial H. ^{57}Fe Mössbauer spectroscopic measurements for both the average magnetic moment and the effective hyperfine field H_{eff} of iron showed an increase in the magnitudes of these two quantities upon hydrogen insertion, without specifically assigning a role for each one of the two iron sites. Further an anisotropic structural change accompanies the formation of the hydride: c/a ($ScFe_2$) = 1.636 and c/a ($ScFe_2H_2$) = 1.611 [3].

In this work hydrogen insertion effects within $ScFe_2$ are examined, using the framework of the density functional theory (DFT) [14–16], within four complementary approaches relevant (i) to the magnetovolume effect due to the volume expansion which should lead to an enhancement of the localization of the iron 3d states due to the reduced d–d overlap, (ii) to the interactions between the valence states of scandium and iron (at both sites) with hydrogen, (iii) to the crystal anisotropy occurring upon the hydrogenation of the alloy system and (iv) to the different roles played by the two Fe sublattices through their specific magnetic moments and the Fermi contact H_{FC} term of the effective hyperfine field. Further, a detailed atom-resolved study of the magnetism is provided and the nature of the non-rigid-band behavior within $ScFe_2$ and its dihydride is assessed.

2. Computational methodology

In the last two decades, several methods of computation for the electronic structure of materials from first principles were built within the density functional theoretical (DFT) framework [14–16]. They play different roles as to the type of problem needing to be solved. Here, two methods are employed. As far as accurate starting geometries were sought, a pseudo-potential (PP) approach was firstly used. Then in order to obtain reliable quantities as to the electronic and magnetic band structures as well as to probe core states for discussing the hyperfine field properties, an all-electrons method was used. These methods are shortly discussed below.

2.1. Pseudo-potential geometry optimizations

In the plane wave pseudo-potential (PP) approach, the rapid variation of the potential near the nuclei is avoided by substituting the all-electrons Hamiltonian with a smoother pseudo-

Hamiltonian which reproduces the valence energy spectrum. As a matter of fact, the use of pseudo-potentials allows a considerable reduction of the necessary number of plane waves per atom for transition metals and first row elements, thus force and full stress tensor can be easily calculated and used to relax atoms into their ground state. This is built within the VASP code with ultra-soft PP [17]. The conjugate-gradient algorithm [18] is used in this computational scheme to relax the ions of the different structural setups of $ScFe_2$ and $ScFe_2H_2$ Laves phases. The exchange–correlation effects are accounted for within the local density approximation (LDA) [19]. The optimization of the structural parameters is performed until the forces on the atoms are less than 0.02 eV/Å and all stress components are less than 0.003 eV/Å^3. All the calculations were performed by using an energy cut-off of 436.75 eV for the plane wave basis set. The tetrahedron method with Blöchl corrections [20] as well as a Methfessel–Paxton scheme [21] for conducting systems were applied for both geometry relaxation and total energy calculations. Brillouin-zone integrals were approximated using the special **k**-point sampling of Monkhorst and Pack [22] with a starting mesh of $4 \times 4 \times 4$ up to $8 \times 8 \times 8$ for best convergence and relaxation to zero strains. From the outputs, energy as a function of volume curves are plotted. From these, quantities such as the equilibrium volume and the bulk modulus can be extracted which are essential to study the compressibility of the intermetallic and its hydride.

2.1.1. Mapping schemes of electron distribution

Further, from PP calculations a mapping of the electrons within the lattice can be obtained. This provides an insight into the charge density distribution as well as into the localization of electrons around the chemical constituents. The latter quantity which meets better the view of the chemist of bonding in systems is the electron localization function (ELF) introduced by Becke and Edgecombe [23,24]. It allows determining the amount of localization of electrons with respect to the free electron gas distribution. This function is described as follows:

$$\mathrm{ELF}(\mathbf{r}) = \frac{1}{1 + [D(\mathbf{r})/D_h(\mathbf{r})]^2},$$

where $D(\mathbf{r})$ represents the density of the local electronic kinetic energy due to the Pauli repulsion and $D_h(\mathbf{r})$ is the density of the kinetic energy of Thomas–Fermi. The latter is given by electron pairs with the same spin orientation within the uniform electron gas which has the same density as the real system at the point defined by the vector $\mathbf{r}$. $D_h(\mathbf{r})$ is represented by the following equation:

$$D_h(\mathbf{r}) = \frac{3}{10}\left(3\pi^2\right)^{3/2}(\rho(\mathbf{r}))^{5/3}$$

with $\rho(\mathbf{r}) = \sum_{i=1}^{N} |\varphi_i(\mathbf{r})|^2$, where φ_i are the Hartree–Fock or the Kohn–Sham orbitals. The dimensionless ELF magnitude ranges from 0 to 1 with ELF = 1/2 corresponding to the free electron gas distribution. These three extreme situations will be illustrated by three sets of colors: ELF = 0 points to no localization (blue contours), ELF = 1 points to strong localization (red contours) and ELF = 1/2 is shown with green contours (cf. Fig. 3(a) and (b)). (For interpretation of the references to color in the text, the reader is referred to the web version of this article.)

2.2. All-electrons calculations

The all-electrons calculations are equally DFT-based with an alternative LDA [25] scheme. They were performed with the augmented spherical wave (ASW) method [26,27] which was successfully used for intermetallic systems in recent years [28–30]. In ASW method, the wave function is expanded in atom-centered augmented spherical waves, which are Hankel functions and numerical solutions of Schrödinger's equation, respectively, outside and inside the so-called augmentation spheres centered on the atomic sites. For the minimal basis set, we chose the outermost shells to represent the valence states and the matrix elements were constructed using partial waves up to $l_{\max.}+1=3$ for Sc and Fe and $l_{\max.}+1=2$ for H. It needs to be said that calculations are started for neutral atom configurations. They are ab inito and self-consistent with increasing **k**-points' precision in the hexagonal Brillouin zone. Convergence is obtained when negligible variations for the charges ($\Delta Q=10^{-8}$) and for the total energy ($\Delta E=10^{-8}$ Ryd), are observed between two successive iterative cycles. In order to optimize the basis set, additional augmented spherical waves were placed at carefully selected interstitial sites (IS). The choice of these sites as well as the augmentation radii was automatically determined using the sphere-geometry optimization algorithm [31]. Self-consistency was achieved by a highly efficient algorithm for convergence acceleration [32]. The Brillouin-zone integrations were performed using the linear tetrahedron method with up to 576 and 1024 **k**-points within the irreducible wedge [20,27] for $ScFe_2$ and $ScFe_2H_2$, respectively.

2.2.1. Accounting for the different magnetic configurations

It is worth mentioning that the all-electrons ASW method was used in complementarity with PP approach for its capacity to evaluate the core charge density needed for the assessment of the Fermi contact term of the hyperfine field as measured for instance by Mössbauer spectroscopy. The computational procedure follows a protocol through which a non-magnetic (NM) configuration is firstly assumed, meaning that spin degeneracy is imposed for all valence states with equal spin occupations, these calculations are also called non-spin polarized (NSP). Such a configuration should not be confused with that of a paramagnet, which could be simulated either by supercell calculations with random spin orientations on atoms, or by calling for disordered local moment approaches based on the coherent potential approximation [33] or the LDA + DMFT (dynamic mean field theory) scheme [34]. Such NM computations are relevant at two levels, allowing to carry out an analysis of the partial atom projected densities of states (PDOS) at the Fermi level with respect to magnetic instability and assessing the chemical bonding. Then spin polarized (SP) calculations with different initial spin populations $\uparrow$ (majority spins) and $\downarrow$ (minority spins) can lead at self-consistency either to finite or zero local moments within an implicit long-range ferromagnetic order. Antiferromagnetic (AFM) calculations can also be done if there is a need to look for an AFM ground state. This can be done by defining half of the atomic constituents as UP spin-aligned and the other half as DOWN spin-aligned, either within the unit cell or by using supercells [35].

2.2.2. Chemical bonding properties

The results obtained from DFT-based calculations provide accurate indications to quantities such as the magnitudes of the magnetic moments, the nature and energy position of the states with respect to the Fermi level (E_F), the ground state configuration from relative energies…. However, the solid state chemist needs a tool to illustrate information about the nature of the chemical bond between two atomic constituents. This can be provided from different available

schemes, such as the crystal orbital overlap population (COOP) [36], the crystal orbital Hamiltonian population (COHP) [37] or the covalent bond energy (ECOV) [38] criteria.

In order to answer the basic question, ''*where are the electrons*?'', Roald Hoffmann introduced the COOP in early extended-Hücke type calculations [36]. This criterion is based on the overlap population (OP):

$$c^*_{ni}(\mathbf{k})S_{ij}c_{nj}(\mathbf{k}) = c^*_{ni}(\mathbf{k})\langle\chi_{ki}(\mathbf{r})|\chi_{kj}(\mathbf{r})\rangle c_{nj}(\mathbf{k}),$$

where S_{ij} is an element of the overlap matrix of the valence basis functions and $c_{nj}(\mathbf{k})$ are the expansion coefficients for the n^{th} band. The partial COOP coefficients $C_{ij}(E)$ over two centers i and j are then obtained by integration of the above expression over the Brillouin zone.

$$C_{ij}(E) = C_{ji}(E) = \frac{1}{\Omega_{\text{BZ}}}\sum_n \int_{\text{BZ}} d^3\,k\text{Real}\{c^*_{ni}(\mathbf{k})S_{ij}c_{nj}(\mathbf{k})\}\delta(E-\epsilon_{nk})$$

Ω_{BZ} is the Brillouin zone volume and Dirac δ serves as a counter of states. $C_{ij}(E)$ can be grossly designated as a density of states (DOS) function modulated by the overlap population. The chemical interaction is then labelled as bonding, antibonding or nonbonding according to the sign of the quantity between { } brackets, i.e., respectively, positive, negative and zero.

Although an accurate description of the chemical bond is effectively provided, the antibonding states are often found with unusually high intensity. An alternative is the Hamiltonian based population (COHP) [37] which gives the contribution of a bond to the total energy by introducing the element of the Hamiltonian:

$$H_{ij} = \langle\chi_{ki}(\mathbf{r})|\widehat{H}|\chi_{kj}(\mathbf{r})\rangle$$

thus giving an expression similar to the COOP:

$$\text{COHP}_{ij}(E) = \frac{1}{\Omega_{\text{BZ}}}\sum_n \int_{\text{BZ}} d^3\,k\text{Real}\{c^*_{ni}(\mathbf{k})H_{ij}c_{nj}(\mathbf{k})\}\delta(E-\epsilon_{nk})$$

Both COOP and COHP approaches provide a qualitative description of the bonding, nonbonding, and antibonding interactions between two atoms. A slight refinement of the COHP was recently proposed in the form of ''covalent bond energy'' (ECOV) which combines both COHP and COOP so as to make the resulting quantity independent of the choice of the zero of potential [38]. In the present work, the ECOV criterion was used for the chemical bonding analysis. In the plots, negative, positive and zero magnitudes of the unitless ECOV are indicative of bonding, antibonding, and nonbonding interactions, respectively.

3. Geometry optimization results

3.1. Crystallographic considerations

Like pristine $ScFe_2$, the dihydride crystallizes in the hexagonal C14-type structure (space group $P6_3/mmc$) [3]. In this structure, shown in Fig. 1, iron atoms are in general 2a and in particular 6h Wyckoff positions, Fe1(0, 0, 0) and Fe2(u_{Fe2}, $2u_{\text{Fe2}}$, 1/4) while Sc are in 4-fold particular positions, 4f at (1/3, 2/3, u_{Sc}). Fe2, Sc and Fe1 atoms have an occupancy ratio of 3:2:1. The choices for hydrogen insertion sites were made based on the neutron diffraction

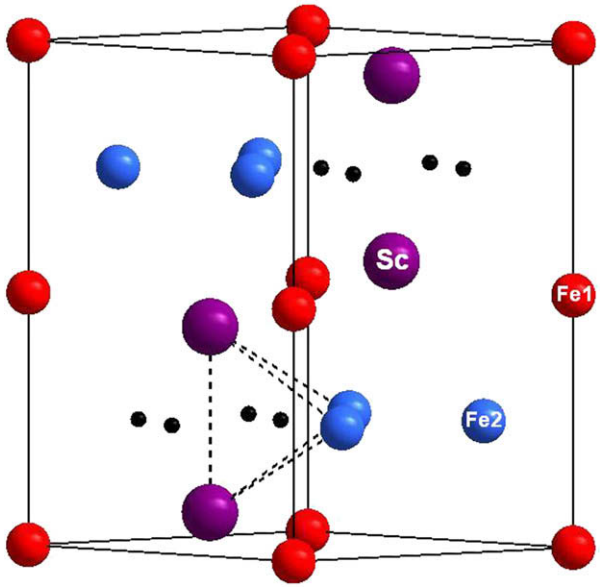

Fig. 1. The hexagonal crystal structure of $ScFe_2H_2$ (C14 Laves phase, space group $P6_3/mmc$). H is represented by small black spheres. Connected dashed lines represent the tetrahedral $A2B2$ H surroundings with two Sc and two Fe2. (For interpretation of the references to color in the text, the reader is referred to the web version of this article.)

studies on the deuterated C14 $ZrMn_2$ [39]. In this system, H atoms occupy interstitial tetrahedral $A2B2$ (A = Sc and B = Fe2) voids with three possible positions: 6h, 12k and 24l which are partially occupied according to the experimental studies. For this reason we carried out preliminary calculations of interatomic distances testing different structural setups with these positions. Similar trends for spacings of H with different sublattices were identified, i.e., $d_{Fe2-H} < d_{Fe1-H}$ (see Table 1). Consequently in the present work, band structure calculations were performed with the assumption that H is located within 6h partially filled sites: H1 at (u_{H1}, $2u_{H1}$, 1/4) and H2 at (u_{H2}, $2u_{H2}$, 1/4) so that the resulting stoichiometry corresponds to the dihydride, $Sc_4Fe_8H_8$. Starting values for a, c as well as the u internal coordinates were taken from experimental data [3,39]. Keeping in mind the relatively large difference in atomic volume between Sc and Fe, the choice of the H insertion sites is in agreement with the Westlake criterion ([40] and therein cited references) that imposes a minimum interstitial hole size of 0.40 Å. Too small H–H distances ($d_{H-H} \geq 2.1$ Å) were avoided in order to respect the Switendick criterion [41] (see Table 1).

3.2. Equilibrium structures and energetics

From the results, the hexagonal symmetry was preserved for both $ScFe_2$ and its hydride. The initial and final u parameters given in Table 1 show slight differences which confirm the assumed setups. In order to obtain the equilibrium volumes and confront them with experiment, (energy, volume) values were computed around the experimental values. The resulting $E(V)$ curves are plotted in Fig. 2(a) and (b) for both $ScFe_2$ and $ScFe_2H_2$ giving equilibrium volumes, respectively, as 40.6 and 47.1 $Å^3$. These are $\sim$6% and $\sim$8% smaller than the experimental

Table 1
Structural results for $ScFe_2$, its dihydride and hydrogen-free $ScFe_2H_2$ models

	$ScFe_2$	H-free $ScFe_2H_2$	H-free $ScFe_2H_2$	$ScFe_2H_2$
	$c/a = 1.636$	$c/a = 1.636$	$c/a = 1.611$	$c/a = 1.611$
a (Å)	4.965	5.250	5.279	5.279
c (Å)	8.125	8.592	8.507	8.507
Volume (Å^3)	40.6/43.4	–	–	47.1/51.3
u_{Sc}	0.066/0.065	–	–	0.066/0.046
u_{Fe2}	0.836/0.828	–	–	0.836/0.830
u_{H1}	–	–	–	0.463/0.462
u_{H2}	–	–	–	0.202/0.212
d_{Sc-Fe1}	2.915	3.084	3.100	3.100
		3.110		
d_{Sc-Fe2}	2.899	3.052	3.068	3.068
	2.952	3.084	3.100	3.100
$d_{Fe1-Fe2}$	2.470	2.592	2.603	2.603
d_{Fe1-H} (Å)	–	–	–	2.800
d_{Fe2-H} (Å)	–	–	–	1.730
d_{Sc-H} (Å)	–	–	–	1.730
d_{H-H} (Å)	–	–	–	2.385
	–	–	–	2.052

Volumes per fu are given as equilibrium/experimental; u internal coordinates are given as starting/final values from the geometry optimization calculations.

volumes which amount to 43.4 and 51.3 Å^3. Such a result is expected within the LDA approximation used, as it is known to under estimate lattice spacings. In order to calculate the bulk modulus B_0 a curve fitting with a Birch third order equation was performed. The obtained magnitudes are 156 and 150 GPa for $ScFe_2$ and $ScFe_2H_2$, respectively. This is indicative of the larger compressibility of the hydride phase, with respect to $ScFe_2$, under hydrostatic pressure. Using the total energy values extracted from the geometry optimization results, one can access the cohesive energy of the hydride system, E_{coh}, which is expressed as follows:

$$E_{coh} = \frac{1}{2}[E(ScFe_2H_2) - E(ScFe_2)] - \frac{1}{2}E(H_2),$$

In this equation, $E(ScFe_2H_2)$ represents the total energy of the hydride system (−118.979 eV), $E(ScFe_2)$ the energy of the intermetallic system (−92.439 eV) and $E(H_2)$ the energy of the dihydrogen molecule (−6.595 eV), the latter being computed by considering a cubic supercell of lattice parameter 4.5 Å. This amounts to a cohesive energy magnitude of −0.02 eV, in favor of a bonded hydrogen within the lattice. Compared with literature, this magnitude of E_{coh} is ∼3 times smaller with respect to $ZrFe_2H_{0.5}$ formation energy [42]. This could point to a more labile H within the scandium based hydride.

3.3. Analysis of electron localization with ELF function

Fig. 3(a) and (b) shows the electron localization function mapping for the planes at $z = 0.25$ and $x = \sim 0.77$. In Fig. 3 the structure and the tetrahedral $A2B2$ void within which hydrogen is inserted are reproduced as in Fig. 1 to enable comparison. The strongest localization is around hydrogen sites while around the Sc and Fe2 locations there is weak localization. This agrees

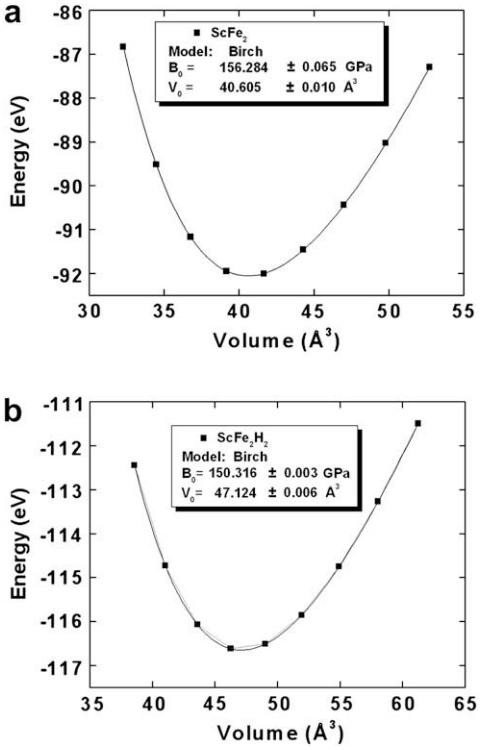

Fig. 2. Energy as a function of cell volume for $ScFe_2$ (a) and $ScFe_2H_2$ (b) showing a larger compressibility of the hydride.

with the "*hydride*" chemical picture of the system, i.e., with negatively charged hydrogen. Between the atomic species the green areas point to a smeared electron distribution within the system similar to a free electron like character expected within a metallic network. From Fig. 3(b) showing the nearest neighbors of hydrogen, the ELF of Sc and Fe2 is seen distorted towards H. This is due to the interactions between Sc and Fe2 on one hand and H on the other hand. This is concomitant with the interatomic distances listed in Table 1 as far as Sc and Fe2 have the shortest separations with H. This issue will be further developed within the chemical bonding section.

4. All-electrons calculations

The crystal parameters provided by the geometry optimization initial processing (Table 1) were used for the input of all-electrons calculations. For $ScFe_2H_2$, the positions of the lacking hydrogen atoms within the 6h interstices were considered as interstitial sites where augmented spherical waves were placed. The resulting breaking of initial crystal symmetry was accounted for from the differentiation of the crystal constituents in the calculations. Since both $ScFe_2$ and $ScFe_2H_2$ systems are experimentally known to have a magnetic behavior, spin polarized calculations (spin-only) were carried out. Further, other sets of computations were performed for hydrogen-free models, at the same volume of the

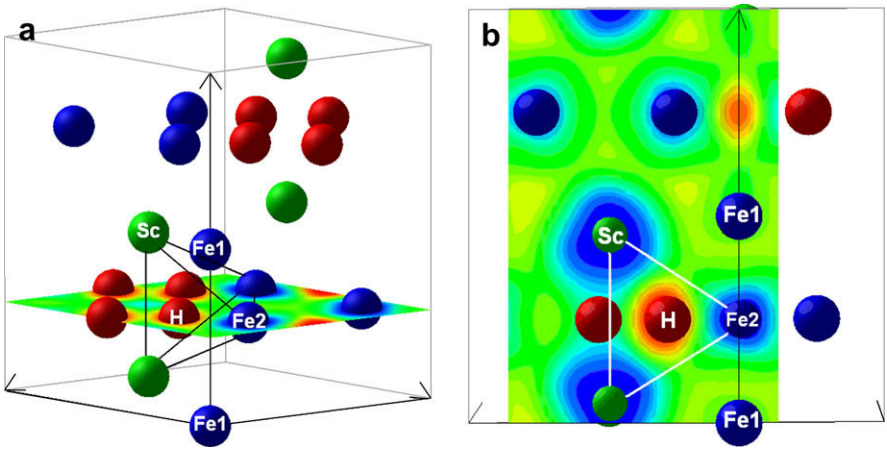

Fig. 3. $ScFe_2H_2$: electron localization function (ELF) maps along the planes $z = 0.25$ (a) and $x = \sim 0.77$ (b). All Fe1 atoms are labeled to differentiate them from Fe2 atoms. Connected full lines represent the tetrahedral H surroundings of two Sc and two Fe2. (For interpretation of the references to color in the text, the reader is referred to the web version of this article.)

experimental hydride [3]. This simulates the manner in which the volume expansion (negative pressure) affects the magnetic behavior of the different atomic species. These effects can be important in such intermetallic systems as far as the onset of the magnetic moment is due to interband spin polarization, i.e., it is mediated by the electron gas in a collective electrons approach. This is opposite to other systems, such as insulating oxides where the magnetization is of intraband character, and hence, is less affected by volume changes such as those induced by pressure [35]. For the sake of addressing anisotropy effects, an additional expanded hydrogen-free $ScFe_2$ model was calculated with the experimental value of the *c*/*a* ratio of the alloy system.

4.1. Spin degenerate calculations

A slight charge transfer of ~ 0.104 electron is seen from Fe2 towards Sc and Fe1. However, its amount is not significant of an ionic behavior – rarely observed in the framework of ab initio calculations for such systems [43]. Therefore it can be argued that the bonding is not mainly due to charge transfer but rather imposed by the hybridization between the different valence states.

4.1.1. Discussing the density of states

The PDOS for $ScFe_2$ and its dihydride are given in Fig. 4(a) and (b) with respect to occupancy ratios given in Section 3.1. This is applied for all the other PDOS panels in this work. Energy reference is with respect to the Fermi level E_F. This is equally followed in all other plots. Looking firstly at the general shape of the PDOS within Fig. 4(a), one can observe that Fe1 and Fe2 curves cross the Fermi level with a predominance in terms of intensity for Fe2 states, i.e., with respect to very low intensity scandium states. The similar skylines between the partial PDOS pointing to the mixing between Fe2, Fe1 and Sc states can be seen at the lower part of the valence band (VB), with mainly s, p like states between -6 and -2.5 eV, as well as

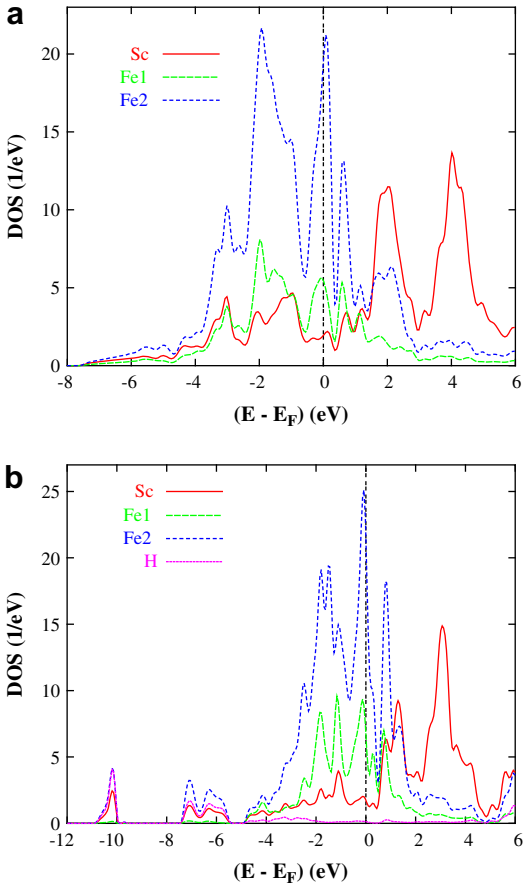

Fig. 4. Non-magnetic site projected DOS of $ScFe_2$ (a) and $ScFe_2H_2$ (b).

towards the top of VB (d states). Such mixing will be analyzed later with the chemical bonding. Lastly, within the conduction band (CB), 3d(Sc) states are found dominant. This is expected as scandium is located at the very beginning of the 3d period, with mainly empty d states.

A visual inspection of Fig. 4(b) allows to establish similar trends with respect to the alloy. Narrower and more localized peaks are found within the energy range [−5 eV, E_F]. These are due to reduced p−d overlap between the Sc, Fe and Fe1. Further, two additional regions appear within VB, [−5, −8] eV and [−10, −12] eV, respectively. One can observe within these regions a quantum mixing between Sc, Fe2 and H. This is significant of interactions between Sc and Fe2 on one hand and H on the other hand. This is concomitant with the character of the ELF described earlier. It is then expected that Fe1 will have a different magnetic behavior within the hydride with respect to pristine $ScFe_2$ as it is the less interacting species with H.

4.1.2. Analysis of the DOS within the Stoner theory

As far as 3d(Fe, Sc) states were treated as band states by our calculations, the Stoner theory of band ferromagnetism [16] can be applied to address the spin polarization. The total energy of

the spin system results from the exchange and kinetic energies counted from a non-magnetic state. Formulating the problem at zero temperature, one can express the total energy as

$$E = \frac{1}{2}\left[\frac{m^2}{n(E_F)}\right][1 - In(E_F)].$$

Here I is the Stoner exchange integral, which is an atomic quantity that can be derived from spin polarized calculations [44]. $n(E_F)$ is the PDOS value for a given species at the Fermi level in the non-magnetic state. The product $In(E_F)$ from the expression above provides a criterion for the stability of the spin system. The change from a non-magnetic configuration towards spin polarization is favorable when $In(E_F) \geq 1$. The system then stabilizes through a gain of energy due to exchange. From Ref. [44], I(Fe) $\sim$ 0.4624 eV and the calculated $In(E_F)$ values of Fe1 and Fe2 are given in Table 2 for all the computed models. These amount to a magnitude of $\sim$1.409 and 1.519 for Fe1 and Fe2, respectively, within $ScFe_2$ on one hand and $\sim$1.645 and 1.799 for Fe1 and Fe2, respectively, within $ScFe_2H_2$. This points to a magnetic instability of both systems. This prediction is concomitant with the experiment [3] where both $ScFe_2$ and $ScFe_2H_2$ are found to be magnetic with an average magnetic moment measured for iron. From the spin polarized calculations, finite magnetic moments are expected to be carried by both Fe1 and Fe2. Also, Table 2 gives the values of the Stoner product for hydrogen-free models. For these, the magnitudes of the Stoner products are found to be larger with respect to the alloy and the dihydride models, indicating a tendency towards magnetic order, which emphasizes an interplay of magneto-volume versus H chemical bonding effects. This will be quantitatively discussed within the spin polarized calculations section where magnitudes of the magnetic moments and the spin occupation of the 3d(Fe1, Fe2) will be presented.

4.1.3. Chemical bonding from pair interactions

The analysis of the chemical bonding is done using the ECOV approach. The corresponding plots for pristine $ScFe_2$ and its dihydride are shown in Fig. 5(a) and (b), respectively. Partial ECOV is given for the atomic pair interactions of Sc–Fe1, Sc–Fe2 and Fe1–Fe2 bonds; this is

Table 2
Magnetic results for $ScFe_2$, its dihydride and hydrogen-free $ScFe_2H_2$ models

	$ScFe_2$	H-free $ScFe_2H_2$	H-free $ScFe_2H_2$	$ScFe_2H_2$
	$c/a = 1.636$	$c/a = 1.636$	$c/a = 1.611$	$c/a = 1.611$
$In(E_F)$	1.409/1.519	1.794/1.914	1.931/1.923	1.645/1.799
E_{rel}	0.000/−0.215	2.560/1.906	2.598/1.917	−24.318/−24.754
m_{Sc}	−0.482	−0.676	−0.682	−0.347
m_{Fe1}	1.468	2.229	2.279	2.486
m_{Fe2}	1.560	2.101	2.118	1.967
$\langle m_{Fe} \rangle$	1.514	2.165	2.198	2.226
M	2.600	3.591	3.635	3.791
H_{FC}^{total}(Fe1)	−157	−240	−246	−203
H_{FC}^{total}(Fe2)	−162	−229	−226	−232
H_{FC}^{core}(Fe1)	−159	−252	−255	−272
H_{FC}^{core}(Fe2)	−164	−232	−231	−214

$In(E_F)$ magnitudes are given for Fe1/Fe2 sublattices, respectively. Given in units of eV, E_{rel} represents the NSP/SP energies per fu of the models with respect to the non-magnetic energy of the alloy ($E_0 = -89859.40896$ eV). Magnetic moments' magnitudes are given in μ_B. Fermi contact term H_{FC} of hyperfine field and its core part H_{FC}^{core} are given in kGauss.

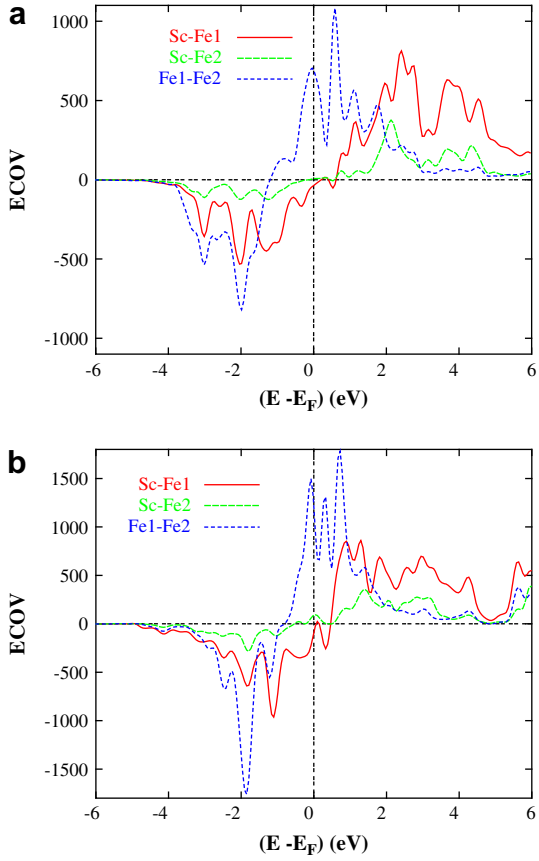

Fig. 5. Chemical bonding: non-magnetic ECOV for $ScFe_2$ (a) and $ScFe_2H_2$ (b).

followed for all ECOVs within this work. In both cases Fe1–Fe2 interaction is found to have the largest bonding peak between −4 eV and −1 eV. This feature is mirrored by an antibonding peak at the top of VB up to E_F which points to the instability of the system in the non-magnetic configuration. Then it can be suggested that the strongest bonding interaction within VB arises from Sc–Fe1, followed by weakly bonding Sc–Fe2. These contribute to the stability of both systems, respectively. The change in bonding strength is proportional to the distance magnitudes given in Table 1, i.e., the shortest interatomic distances characterize the strongest interactions. This applies for the Sc–Fe1 and Sc–Fe2 interactions as far as $d_{Sc-Fe1} < d_{Sc-Fe2}$ for both alloy and its dihydride. Further, one can notice that the electrons in the d band crossed by the Fermi level for Sc–Fe1 and Sc–Fe2 interactions, are not all antibonding. A part of those electrons become nonbonding in the neighborhood of E_F, thus participating in the onset of the magnetic moment. This is expected for iron as far as the experiment determines magnetic $ScFe_2$ and $ScFe_2H_2$. We also suggest the possibility of an ordered magnetic moment to be carried by Sc, since it takes part in both nonbonding interactions at E_F. This proposition will be examined within the spin polarized calculations as a finite moment is expected for Sc.

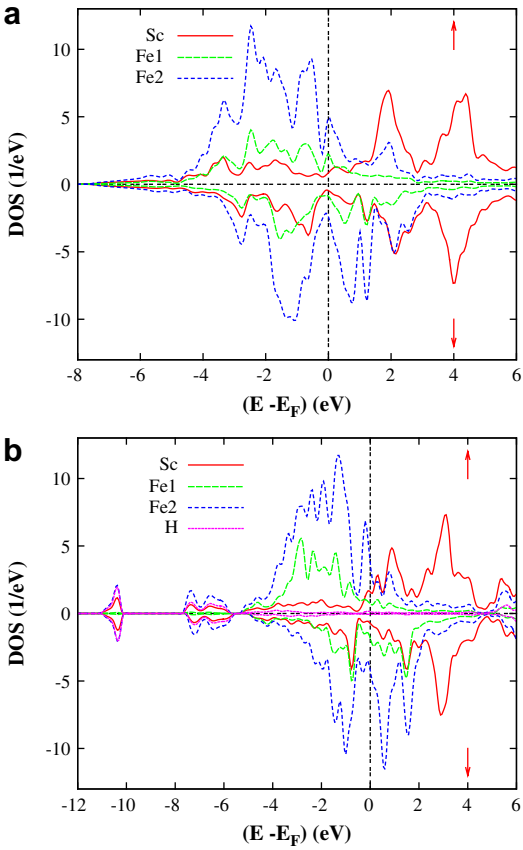

Fig. 6. Site and spin projected PDOS of $ScFe_2$ (a) and $ScFe_2H_2$ (b).

4.2. Spin polarized SP calculations

As it can be expected for the spin polarized configuration of all models (see Table 2), there is an energy stabilization with respect to the non-spin polarized configuration. This agrees with the experimental data whereby $ScFe_2$ and its dihydride are identified, both magnetically ordered as ferromagnets [13,45,46]. On the other hand, the relative energies' (E_{rel}) magnitudes, which represent the difference between NSP or SP energies and the non-magnetic energy of the alloy ($E_0 = -89859.40896$ eV), indicate that the magnetic configuration of the hydride system is the most stable. Further, both expanded H-free models are unstable. This can be expected as far as such hypothetical systems were not evidenced by the experiment.

4.2.1. Site and spin projected density of states

The PDOS curves for the spin polarized configuration of $ScFe_2$ are shown in Fig. 6. Within the VB two energy regions can be identified, from -7.5 to -5 eV, low intensity itinerant s, p states of all constituents are found; this is followed by larger intensity peaks mainly due to 3d(Fe) up to and above E_F. Exchange splitting can be seen to mainly affect the latter as it is

expected from the above analysis of the magnetizations. Majority ↑-spin states, for both Fe1 and Fe2 at E_F, are concentrated in sharp and narrow PDOS peaks, contrary to minority ↓-spin states that are found in PDOS minima. Fe1 and Fe2 peaks within the energy range [−1.3, −0.3] eV for ↑-spin states are similar to those corresponding to [0, 1] eV for ↓-*spin* states. This shift in spectral weight for ↑-spin states below the Fermi level and for ↓-spin states above E_F corresponds to the onset of magnetic moments carried by Fe1 and Fe2. One can attribute this to a Stoner rigid-band magnetism at first sight. But PDOS weights for ↑- and ↓-spin populations are not the same. This mismatch between both spin populations is mainly due to the 3d(Fe2) state peaks at ∼1 eV for the ↓-spin states. One also notices that the peaks at ∼−0.7 eV for ↓-spin 3d(Sc) states are more intense than those for ↑-spin states. This graphical feature points to the possibility of a magnetic moment carried by Sc with and opposite direction to those carried by Fe1 and Fe2. The moment of scandium is provided by the covalent Sc−Fe1 bond, rather than by a rigid energy shift of non-magnetic PDOS, whence its negative sign − notice the Sc−Fe1 overlap around −0.7 eV for ↓-spin PDOS.

4.2.2. Covalent magnetism approach of the DOS

Generally, the magnetism of metals and alloys is correctly provided within the Stoner model [16] whereby the magnetic moment is the result of a rigid-band shift of an initially non-magnetic (i.e., with total spins) system to low energy majority-spin (↑) DOS below the Fermi level and to minority-spin (↓) DOS at higher energy (above E_F). This is the case of body centered cubic ferromagnetic α-Fe. However, early magnetic band calculations [47] allowed to identify a new feature exhibited by many intermetallic systems such as $ZrFe_2$ [48], where the weights of the two spin populations' DOS are not equal as proposed by the Stoner rectangular rigid-band model. The model of ''covalent magnetism'' was therefore proposed to provide an explanation going beyond the basic Stoner model. Schematically, the model borrows the concept of chemistry, by using a molecular orbital type sketching of the way spins of two magnetic species arrange in the lattice [49]. The result is a larger majority DOS weight with respect to the minority DOS on one hand and different partial DOS (PDOS) intensities in the spin down channel, on the other hand. Interestingly our systems under investigation are described in this framework too.

4.2.3. $ScFe_2$ and magnetovolume effects

Magnetic moments are obtained from the charge difference between ↑-spin and ↓-spin of all valence states; their calculated values are listed in Table 2. The computed magnitudes for both the average magnetic moment of iron and the magnetization per fu for $ScFe_2$ are 1.514 and 2.600 μ_B, respectively. These are within the range of the experiment [46], where magnitudes of 2.9 and 1.45 μ_B are measured for the average magnetic moment of iron and the magnetization per fu, respectively. Also Sc carries a negative magnetic moment of −0.482 μ_B. Thus $ScFe_2$ is closer to a ferrimagnet than to a ferromagnet suggested by experimental results [3,13]. The same feature of antiparallel magnetic alignment between the two constituents was equally observed for YFe_2 [43]. Moreover, the 3d(Sc) states have a calculated value of −0.347 μ_B which stands out as the largest contribution within the magnetic moment. The second largest contribution is that of the 4p(Sc) states with a value of −0.103 μ_B. The magnitude of the average magnetic moment for iron within $ScFe_2H_2$ is of 2.226 μ_B in agreement with experimental value of 2.23 μ_B [3]. This computed value corresponds to an increase of 67% with respect to $ScFe_2$. The volume expansion induces an increase in the average magnetic moment of iron as seen for the expanded H-free model in Table 2.

4.2.4. $ScFe_2H_2$ and the role of hydrogen

At self-consistent energy convergence, little charge transfer (±0.1 electron) is observed between the atomic species. It results from a charge redistribution due to the overlapping between the valence states of atomic constituents. Thus there is no significant ionic behavior such as the description of the system as a "*hydride*" from the chemistry point of view as it was argued in earlier works on YFe_2H_x systems [43]. In fact the major issue for understanding the actual chemical system is through the discussion of the site and spin projected density of states (PDOS) because they describe the relative energy positions of the different valence states. The PDOS accounting for site multiplicities within $ScFe_2H_2$ are shown in Fig. 6(b). In comparison with the pristine intermetallic system $ScFe_2$ (cf. Section 4.2.1), the VB of the hydride is 4 eV wider. Consequently, the energy intervals given above are found here too with the difference of widened itinerant part which now includes H s-like states, i.e., [−11, −6] eV. The similar skylines between the PDOS of the different atomic species in the energy regions describe the hybridization of the metallic species with hydrogen. The sharper and narrower nature of these PDOS peaks, compared to those of $ScFe_2$ (see Fig. 6(a)), points to a larger localization of the states in the hydride system. In particular, one can notice a sharper localization of Fe1 PDOS, within the energy range between −5 eV and E_F, where the PDOS magnitude falls to ∼0, while the PDOS for Fe2 has a finite magnitude at E_F. This feature is significant of peculiar magnetic behaviors of the two Fe sublattices.

4.2.5. Strong and weak ferromagnetism within $ScFe_2H_2$

Within the hydride $ScFe_2H_2$, hydrogen insertion is seen to further increase the average moment magnitude. But looking at the relative magnitudes of the iron magnetic moment there is an interesting feature relevant to the inversion of magnitudes for Fe1 and Fe2 magnetic moments, i.e., 2.486 and 1.967 μ_B, respectively. This can be due to the closer Fe2−H (1.73 Å) separation than Fe1−H (2.8 Å) one as it will be further analyzed in the spin resolved chemical bonding section. Nevertheless, this pertains to relevant physics of magnetism which is obtained from a detailed analysis of the electron populations. Considering the majority spins (↑), there is close amount of charge distribution in both Fe d states within the pristine alloy system, i.e., $3d^{4.05}_{Fe1}$ and $3d^{4.07}_{Fe2}$. Turning to the dihydride, this is no more the case and these populations become unbalanced, i.e., $3d^{4.6}_{Fe1}$ and $3d^{4.3}_{Fe2}$. An electron population close to 5 for Fe1-d(↑) corresponds to a nearly half-filled d band while this is not so for Fe2. One can further confirm this trend by simulating a hypothetical tri-hydride $ScFe_2H_3$ by filling up all interstitial 6h positions. The resulting majority spin populations are found increasingly unbalanced, with $3d^{4.8}_{Fe1}$ and $3d^{3.7}_{Fe2}$; for minority spins these numbers are such as $3d^{1.8}_{Fe1}$ and $3d^{3.3}_{Fe2}$. The resulting magnetic moments for Fe1 and Fe2 are ∼3 and 0.4 μ_B, respectively. A lowering of the overall magnetization, i.e., 1.95 versus 3.79 μ_B is then obtained. This can be explained by an increasingly − magnetically − isolated Fe1 with respect to Fe2 which loses its spins by pairing with neighboring 12 H. This particular situation is found in magnetic systems which present simultaneously strong and weak ferromagnetic constituents such as the perovskite-like iron nitride γ-Fe_4N [50]. In this system Fe atoms which are close to N at face centers behave as weak ferromagnets with $M(Fe_{fc}) = 2\ \mu_B$, while those away from N at cube corners behave as strong ferromagnets with an enhanced magnetic moment, $M(Fe_c) = 3\ \mu_B$. A strong ferromagnet in this definition has a completely filled subband, here d(↑) and the Fermi level falls to a DOS minimum; this is also observed from the Fe1 PDOS in Fig. 5(b). As a consequence the hydride is characterized by the simultaneous presence of strongly and weakly magnetic behaving iron

species, Fe1 and Fe2, respectively. We emphasize that this is a known feature characterizing *INVAR* alloy, $Ni_{0.35}Fe_{0.65}$ as well (Ni,Pd)Fe_3N nitrides [51].

4.2.6. The Fermi contact term of the hyperfine field

Another significant result extracted from these calculations is the Fermi contact term of the hyperfine field (H_{FC}) (see Table 2). The effective magnetic field H_{eff} acting on a nucleus is considered as the sum of four contributions; (i) H_i, the internal field which is the magnetic field at the nucleus generated from an externally applied field, (ii) H_{FC}, the Fermi contact term, based on the spin density at the nucleus for the *ns* quantum states caused by the polarization of the s electrons and by the d moments, (iii) H_{orb}, which is the field arising from the orbital magnetic moment and (iv) H_{dip}, representing the dipole interaction with the surrounding atoms. In a non-relativistic description, H_{FC} is expressed by the formula:

$$H_{FC} = -\frac{8\pi}{3}\gamma_N\{(\Phi_\uparrow(0))^2-(\Phi_\downarrow(0))^2\},$$

where γ_N is the nuclear gyromagnetic ratio and the quantities between brackets are the densities of s electrons at the nucleus ($r=0$) for $\uparrow$- and $\downarrow$-spins, respectively. The calculations for intermetallic $ScFe_2$ provided H_{FC} magnitudes of -157 and -162 kGauss for Fe1 and Fe2, respectively. ^{57}Fe Mössbauer spectroscopic works reported experimental magnitudes for H_{eff} [3] such as -167 and -174 kGauss without assigning them to the corresponding iron site. The computational results permit to establish the following tendency by assigning the former magnitude to Fe1 and the latter to Fe2. As for the difference with respect to the experiment, it can be related to different origins relevant to (i) drawbacks of the LDA in treating with sufficient accuracy the polarization of core wave functions [52], and (ii) the non-stoichiometry of the experimentally prepared alloys and the subsequent disorder within the solid solutions.

4.2.7. Discussion of core and valence components of H_{FC}

The calculated H_{FC} magnitudes for the hydride system are -203 and -232 kGauss for Fe1 and Fe2, respectively. Experimental findings [3] point to magnitudes of -239 and -300 kGauss for H_{eff}. These experimental values were not assigned to the different iron sites. Before doing so, one must treat the striking feature of the large departure from experimental values. It is thus suggested to decompose H_{FC} into its major contributions namely the one arising from the core 1s, 2s and 3s electrons (H_{FC}^{core}) and the one from the valence 4s electrons (H_{FC}^{val}) [50]. While H_{FC}^{core} is usually strictly proportional to the magnetic moment, H_{FC}^{val} contains large contributions from the neighboring atoms. The calculated H_{FC}^{total} values presented within this work are the sum of these two parts. Since Fe1 interacts weakly with other constituents, its contact with them is reduced. Consequently only the core contribution of H_{FC} must be considered for Fe1. In contrast, Fe2 atoms' interactions with neighboring species are larger, hence both core and valence contributions of H_{FC} must be accounted for. The computed value of H_{FC}^{core} for Fe1 results into a magnitude of -272 kGauss. Now a comparison can be established between the computed core and total H_{FC} magnitudes of -272 and -232 kGauss for Fe1 and Fe2, respectively, on one side and the experimentally measured magnitudes of -300 and -239 kGauss on the other side. It follows that the largest experimental value of -300 kGauss for H_{eff} can be assigned to Fe1 and the smallest value of -239 kGauss is assumed for Fe2. Also, the orders of magnitudes for H_{FC} (see Table 2) are proportional to that of the magnetic moments in both $ScFe_2$ and $ScFe_2H_2$. Thus the inversion of the order of magnitudes is also observed for the hyperfine field.

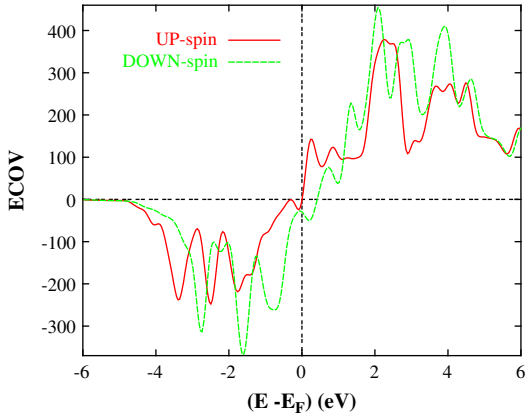

Fig. 7. Spin resolved chemical bonding: ↑ and ↓ ECOV-spin for Sc–Fe1 atomic pair interaction within $ScFe_2$.

4.2.8. Spin resolved chemical bonding

Magnetic quantities such as the ordered magnetic moments' signs and magnitudes and the hyperfine field, can be illustrated by the chemical interactions between the different constituents. A better understanding of the former is thus correlated to a good description of the latter. Within this work, many novel features are shown such as the scandium negative magnetic moment, the inversion of the order of the moments' magnitudes for the dihydride with respect to the alloy system and the account for the core contribution of H_{FC} for Fe1 while both core and valence are considered for Fe2. Fig. 7 shows Sc–Fe1 interactions for ↓- and ↑-spin states' curves for $ScFe_2$. These are responsible for the magnetic moment carried by scandium which was announced earlier on within the non-magnetic ECOV section. One can notice that ↓-spin interaction is the strongest, explaining thus the negative sign of the moment carried by Sc. In particular, the peak at ~ -0.7 eV is concomitant with the overlap between 3d Sc and Fe1 states shown in Fig. 6 for the spin polarized PDOS within the alloy system.

On the other hand, the different Fe–H interactions are resolved for the two spin orientations as shown in Fig. 8(a) and (b), these are plotted for all atoms contrary to the other ECOV where atom to atom interactions are sketched. Fe1 interactions with hydrogen are weak with a slightly antibonding character shown in Fig. 8(a) (majority spins) and negligible bonding magnitude shown in Fig. 8(b) (minority spins) within the VB. The second less weak bonding is the Sc–H one; it is bonding throughout the VB in both panels. But the major contribution to the bonding comes from strong Fe2–H bonds in both panels. These results illustrate the discussion in earlier sections for the inversion and the hyperfine field. This is in agreement with the interatomic distances given in Table 1 which shows shorter Sc–H and Fe2–H separations with respect to Fe1–H. Thus it can be considered that the Fe1 sublattice is shielded from the other atomic species by hydrogen atoms.

4.3. $ScFe_2$ and anisotropy changes

For the sake of addressing anisotropy effects, an additional expanded hydrogen-free $ScFe_2H_2$ model was calculated with the experimental value of the *c*/*a* ratio of the alloy system [3]. The computed magnitudes and signs for the magnetic moments as well as for H_{FC} are

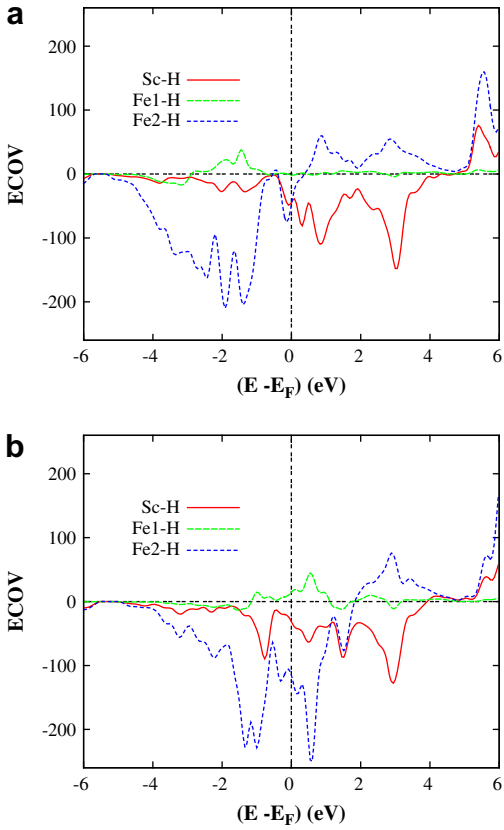

Fig. 8. $ScFe_2H_2$: bonding with ECOV criterion for metal–H ↑-spin interactions (a) and ↓-spin interactions (b).

reported in Table 2. An analysis of these results demonstrates that the change of the *c/a* ratio does not affect the general trends of the magnetic behavior. Moreover, the already observed inversion (upon volume expansion) for the order of magnitudes for both magnetic moments and H_{FC} is conserved. It can be then concluded that the anisotropy changes are of negligible influence on the magnetic behavior of $ScFe_2H_2$, i.e., with respect to both volume expansion and hydrogen insertion effects.

5. Conclusions

In this work local spin density functional (LSDF) investigations of the hydrogen insertion effects on the magnetism and bonding within the C14 $ScFe_2$ Laves phase have been undertaken. As far as no experimental data were available for the particular positions for scandium, iron and hydrogen, a geometry optimization was firstly performed by plane wave ultra-soft pseudo-potential calculations. Energy curves as a function of volume were fitted with a Birch equation resulting into equilibrium volumes, and bulk modulus for both $ScFe_2$ and $ScFe_2H_2$. The former quantities, i.e., equilibrium volumes, are found within the range of the experiment, while the latter quantities show that the hydride system is more compressible under hydrostatic

pressure. The results allowed to carry out a direct space analysis of the electron localization showing the expected chemical picture of a ''*hydride*'' system.

While experimental data were available for the magnitudes of both the average magnetic moment of iron and the effective hyperfine field, their non-assignment to the corresponding iron sites led to address these features calling for all-electrons computations using the optimized data for the electronic band structure for the intermetallic system and its hydride. Expanded, isotropic and anisotropic with respect to $ScFe_2$, hydrogen-free $ScFe_2H_2$ models were also calculated to account for both anisotropy and volume expansion effects. Contrary to former studies which described the magnetic behavior of $ScFe_2$ by means of a rigid-band shift, our results point to a ''covalent magnetism''-like behavior already identified by us in other systems. An original feature is brought by volume expansion that of the inversion of the order of magnitudes of the moments for the hydride system with respect to $ScFe_2$, i.e., Fe1 holds a larger moment than Fe2. This inversion is brought by the stronger Fe2–H interaction with respect to Fe1–H and results in an unbalance state of 3d electron occupation between the two Fe sublattices as compared to equally filled ones in the alloy. This is interpreted in terms of a strong ferromagnetic behavior for Fe1 while Fe2 shows weak ferromagnetism. Further, the calculated magnitudes of Fe1 and Fe2 moments compare well with the experiment. Also, a negative magnetic moment was found to be carried by Sc within both $ScFe_2$ and $ScFe_2H_2$. This suggests a ferrimagnetic ordering in contrast to experimentally proposed ferromagnetism. ^{57}Fe Mössbauer spectroscopic works reported experimental magnitudes of the effective hyperfine field H_{eff} for both intermetallic and hydride systems without assigning them to the two iron sublattices. This was achieved by the computations from which the major Fermi contact H_{FC} contribution of H_{eff} was calculated for $ScFe_2$. The resulting values compare with the experiment. The investigation of the hyperfine field for the hydride required a deeper study of the Fermi contact term with respect to the alloy, i.e., both its core and valence contributions were considered. The resulting magnitudes are within range of experimental data. This helped in assigning the experimental effective hyperfine field magnitudes, reported by ^{57}Fe Mössbauer spectroscopic works, to the corresponding iron sublattice. On the other hand, an overview of the computed results shows that the anisotropy changes have no significant effects on the general magnetic behavior. We propose that these results should apply to other C14 Laves phases and their hydrides.

Acknowledgments

Computational facilities were provided within the intensive numerical simulation facilities network M3PEC of the Université de Bordeaux (http://www.m3pec.u-bordeaux1.fr), partly financed by the Conseil Régional d'Aquitaine and the French Ministry of Research and Technology.

References

[1] Laves F. Theory of alloy phases. In: Buschow KHJ, editor. Electronic and magnetic properties of metals and ceramics. Part I, vol. 3A. Cleveland, OH: American Society for Metals; 1956. p. 124.
[2] Constitution diagrams of binary and multicomponent systems based on iron handbook. Moscow: Metallurgiya; 1986.
[3] Smit PH, Buschow KHJ. Phys Rev B 1980;21.
[4] Niarcos D, Viccaro PJ, Dunlap BD, Aldred AT. Hyperfine Interact 1981;9:563.
[5] Semenenko KN, Sirotina RA, Savchenkova AP, Burnasheva VV, Lototskii MV, Fokina EE, et al. J Less Common Met 1985;106:349.

[6] Schlapbach L, Züttel A. Nature 2001;414:353.
[7] Züttel A. Mater Today 2003;6:24.
[8] Boring AM, Albers RC, Schadler GH, Lawso AC, Weinberger P, Christensen NE. Phys Rev B 1987;36:5507.
[9] Konishi T, Mamiya K, Morikawa K, Kobayashi K, Mizokawa T, Fujimori A, et al. J Electron Spectrosc Relat Phenom 1998;88:303.
[10] Bodak OI, Kotur BYa, Gavrilenko IS, Mrkiv VYa, Ivanchenko GI. Dokl Akad Nauk SSSR Ser A 1978;4:366.
[11] Sebastian MT, Narayanan K, Krishna P. Phys Status Solidi 1987;102:241.
[12] Kumar KS, Hazzledine PM. Intermetallics 2004;12:763.
[13] Ishida S, Asano S. J Phys Soc Jpn 1985;54:4688.
[14] Hohenberg P, Kohn W. Phys Rev B 1964;136:864.
[15] Kohn W, Sham LJ. Phys Rev A 1965;140:1133.
[16] Kübler J, Eyert V. Electronic structure calculations in materials science and technology. In: Buschow KHJ, editor. Electronic and magnetic properties of metals and ceramics. Part I, vol. 3A. Weinheim: VCH Verlag; 1992. p. 1–145.
[17] Kresse G, Furthmüller J. Phys Rev B 1996;54:11169.
[18] Press WH, Flannery BP, Teukolsky SA, Vetterling WT. Numerical recipes. New York: Cambridge University Press; 1986.
[19] Perdew JP, Zunger A. Phys Rev B 1981;23:5048.
[20] Blöchl PE. Phys Rev B 1994;50:17953.
[21] Methfessel M, Paxton AT. Phys Rev B 1989;40:3616.
[22] Monkhorst HJ, Pack JD. Phys Rev B 1976;13:5188.
[23] Becke AD, Edgecombe KE. J Chem Phys 1990;92(9):5397.
[24] Becke AD, Edgecombe KE. Nature 1994;371:683.
[25] Vosko SH, Wilk L, Nusair M. Can J Phys 1980;58:1200.
[26] Williams AR, Kübler J, Gelatt Jr CD. Phys Rev B 1979;19:6094.
[27] Eyert V. The augmented spherical wave method – a comprehensive treatment. In: Lecture notes in physics, vol. 719. Berlin, Heidelberg: Springer; 2007.
[28] Chevalier B, Matar SF. Phys Rev B 2004;70:174408.
[29] Eyert V, Laschinger C, Kopp T, Frésard R. Chem Phys Lett 2004;385:249.
[30] Matar SF, Gaudin E, Chevalier B, Pöttgen R. Solid State Sci 2007;9:274.
[31] Eyert V, Höck K-H. Phys Rev B 1998;57:12727.
[32] Eyert V. J Comput Phys 1996;124:271.
[33] Niklasson AMN, Wills JM, Katsnelson MI, Abrikosov IA, Eriksson O, Johannsson B. Phys Rev B 2003;67:235105.
[34] Nekrasov IA, Held K, Blümer N, Poteryaev AI, Anisimov VI, Vollhardt D. Eur Phys J B Condens Matter Phys 2000;18:55.
[35] Matar SF. Prog Solid State Chem 2003;31:239.
[36] Hoffmann R. Angew Chem Int Ed Engl 1987;26:846.
[37] Dronskowski R, Blöchl PE. J Phys Chem 1993;97:8617.
[38] Bester G, Fähnle M. J Phys Condens Matter 2001;13:11541.
[39] Didisheim JJ, Yvon K, Shaltiel D, Fischer P. Solid State Commun 1979;31:47.
[40] Westlake DG. J Less-Common Met 1983;91:275.
[41] Switendick AE. Z Phys Chem NF 1979;117:89.
[42] Hong S, Fu CL. Phys Rev B 2002;66:94109.
[43] Paul-Boncour V, Matar SF. Phys Rev B 2004;70:184435.
[44] Janak JF. Phys Rev B 1977;16:255.
[45] Ikeda K, Nakamichi T, Yamada T, Yamamoto M. J Phys Soc Jpn 1974;36:611.
[46] Sankar G, Wallace WE. Magn Lett 1976;1:3.
[47] Williams AR, Zeller R, Moruzzi VL, Gelatt CD. J Appl Phys 1981;52:2067.
[48] Mohn P, Schwarz K. Physica B 1985;130:26.
[49] Matar SF, Houari A, Belkhir MA, Zakhour M. Z Naturforsch B 2007;62b:881.
[50] Mohn P, Matar SF. J Magn Magn Mater 1999;191:234.
[51] Mohn P, Schwarz K, Matar SF, Demazeau G. Phys Rev B 1992;45:4000.
[52] Richter M. Electronic structure and magnetism of lanthanide, actinide, and transition metal systems. Germany: Technical University of Dresden; 1997.